Journal of Fluorescence (2022) 32:189–202
https://doi.org/10.1007/s10895-021-02839-5

ORIGINAL ARTICLE

A Novel Imidazole Bound Schiff Base as Highly Selective "Turn-on" Fluorescence Sensor for Zn^{2+} and Colorimetric Kit for Co^{2+}

Anjali Krishna Gopalakrishnan[1] · Shanty Antony Angamaly[2] · Savitha Devaswamparambil Pradeep[1] · Dhanya Thaikatt Madhusoodhanan[1] · Divya Kizhakkeppurath Manoharan[1,3] · Puzhavoorparambil Velayudhan Mohanan[1]

Received: 30 August 2021 / Accepted: 18 October 2021 / Published online: 23 October 2021

Abstract

An imidazole based Schiff base (2-[(1H-imidazole-2-ylmethylene)-amino]-4-methyl-phenol) (IMP), with an imine unit, has been designed and characterized by various standard methods. The evaluation of the probe as a fluorogenic sensor for Zn^{2+} and a chromogenic sensor for Co^{2+} has been rationalized in terms of the PET mechanism. In the presence of Zn^{2+}, a light yellow colored solution of IMP with maximum absorption of 364 nm becomes bright yellow with maximum absorption of 410 nm and a measurable fluorescent signal at 612 nm with bathochromic enhancement. The sensitivity of the fluorescent based assay (6.78×10^{-9} M) for Zn^{2+} is far below the limit in the World Health Organization (WHO) guidelines for drinking water (7.6×10^{-5} M) and therefore it is capable of being a practical system for the monitoring of Zn^{2+} concentrations in aqueous samples. Moreover, IMP showed a highly selective colorimetric response to Co^{2+} by displayed an obvious pink color upon addition of metal solution immediately without any interference from other ions. These results provide a new approach for selectively recognizing the two most important trace elements in the human body simultaneously, for Zn^{2+} by emission spectra and Co^{2+} by the naked eye.

Keywords Imidazole · Colorimetric · Fluorogenic · Zn^{2+} · Co^{2+}

Introduction

In recent years, fluorescent molecular sensors for the detection of various metal ions have been an extensive area of research due to several advantages over other techniques [1–3]. A large portion of the metal ions assuming a significant role in an assortment of industrial tasks like food, drug, paper, material, water treatment, assembling of batteries, and electronic field [4–6]. Fluorescence technology was broadly improved from the year 1960s and there has been sensational development in the utilization of fluorescence for cell and atomic imaging that can be seen today in various disciplines. In particular, Schiff bases have excellent coordination environment, which makes them more convenient to be used as a fluorescent probe for the detection of metal ions [7–9]. Schiff base subsidiaries containing nitrogen–oxygen-rich coordination as a receptor site pave an effective medium for fluorescent detection with observable color change [10–12].

Zinc is perhaps the most flexible and essential metal with diverse biological functions like cistron transcription, brain performance, pathology, immune perform, and cell replica [13–15]. Thus, hereditary irregularities prompting the misregulation in the activities of zinc metal may cause various sicknesses like cerebral ischemia, amyotrophic sidelong sclerosis (ALS), Parkinson's illness, and epilepsy [16]. Because of the absence of spectroscopic

✉ Puzhavoorparambil Velayudhan Mohanan
mohan@cusat.ac.in

Anjali Krishna Gopalakrishnan
anjalianju123krishna@gmail.com

Shanty Antony Angamaly
shanty.sheen@gmail.com

Divya Kizhakkeppurath Manoharan
divyadevuty2008@gmail.com

[1] Department of Applied Chemistry, Cochin University of Science and Technology, Kochi-22, Kerala, India

[2] Department of Chemistry, St. Teresa's College, Ernakulam, Kerala, India

[3] Department of Chemistry, NSS College, University of Kerala, Cherthala, Alappuzha, India

marks of Zn^{2+}, it involves incredible significance to create productive recognizing and observing techniques for Zn^{2+} [17]. Fluorescence based recognition is an amazing asset to identify Zn^{2+} due to its high affectability and quick reaction. To date, the number of chemosensors for Zn^{2+} has been developed, but a few of them actually experience issues in distinctive Zn^{2+} from other metals. Therefore, it is desirable to develop a method for monitoring and detecting Zn^{2+}, which would offer a promising approach to study its actions in biological, medical, and environmental circumstances [18].

Cobalt is an essential trace element that is actively involved in the development of vitamin B12 which is also found in specific minerals of the earth's crust [19, 20]. Although a variety of methods, such as atomic absorption spectroscopy [21, 22] chemiluminescence [23, 24], and ICP mass spectrometry [25–27], are widely used to detect cobalt ions, they have disadvantages because of high-cost technic. Hence, the interest for techniques that are straightforward and particular to distinguish cobalt particles is persistently expanding. Among these recognition strategies, a colorimetric technique for the location of metal particles is very much needful. With recent development in technology, the invention of a new small molecular systems as a probe in different forms are developing as an important colorimetric receptors for metal ions [28, 29]. Also, the visual sensing of Co^{2+} over a wide range of transition metal ions using imidazole cored Schiff base is an important method of detection which allows a direct analysis of the substrate [30].

At hand, for these reasons, we report the design, synthesis and spectroscopic characterizations of a novel imidazole bound Schiff base based chemosensor, IMP for selective fluorometric and colorimetric detection of Zn^{2+} and Co^{2+} respectively. The unique combination of imidazole and aromatic phenolic moiety with imine as a bridge results in the excellent coordination to metal ions by providing the dual property of the sensor. Until now, there are no reports on imidazole bound Schiff base sensor can successfully distinguish Zn^{2+} and Co^{2+} by turn-on fluorescence and visual effect. Moreover, it would quantify Zn^{2+} in the water sample appreciated the efficacy of the probe.

Experimental

Reagents and Equipment's

All the solvents (analytical and spectroscopic grade) were retrieved commercially. All the needed chemicals were purchased from Sigma-Aldrich. The stock solutions of various metal ions were prepared from $Zn(OAc)_2{\cdot}H_2O$, NaCl, KCl, $SrCl_2.6H_2O$, $InCl_3$, $MnCl_2$, $Cu(OAc)_2$, $Co(OAc)_2{\cdot}H_2O$, $Hg(OAc)_2$, $NiCl_2{\cdot}6H_2O$, $Pb(OAc)_2{\cdot}H_2O$, $FeCl_2.4H_2O$, $FeCl_3$, $Mg(OAc)_2{\cdot}4H_2O$ and $Cd(OAc)_2{\cdot}H_2O$. The melting point of the synthesized probe was analyzed by an electrical heating method using capillary tubes.

Absorption spectra were recorded at room temperature using Thermo Scientific™ Evolution 201 UV–visible Spectrophotometer. FT-IR spectrum was worked on JASCO-8000 FT-IR spectrophotometer using KBr pellets in the range of 400–4000 cm^{-1}. Elemental analysis of probe was done using an ElementarVario EL III CHN analyzer at Sophisticated Test and Instrumentation Centre (SAIF), Cochin University of Science and Technology, Kochi, India. ^1H (400 MHz) and ^{13}C NMR (100 MHz) spectra were recorded in DMSO-d_6 as the solvent on a Burker Advance DRX 300 FT-NMR spectrometer with TMS as the internal standard. Liquid chromatography–mass spectrometry (LC–MS) was worked on a Waters 3100 Mass Detector using ESI–MS technique at Cochin University of Science and Technology, Kochi, India. Fluorescence measurements were performed on a Horiba Fluorolog3 FL-1057 model fluorescence spectrometer.

Synthesis of IMP

(2-[(1H-imidazole-2-ylmethylene)-amino]-4-methyl-phenol) A solution of Imidazole-2-carboxaldehyde (0.20 g, 2 mmol) in methanol was added slowly to a solution of 2-amino-p-cresol (0.25 g, 2 mmol) in methanol. The reaction mixture was blended for 8 h at 60 °C. The resulting light yellow colored solution was allowed to evaporate at room temperature. Anhydrous ether was added to deposit a yellowish precipitate. The precipitate obtained was washed several times with methanol which was then recrystallized from DMF and then dried in vacuo over anhydrous $CaCl_2$. The purity of the compound was tested with TLC (Hexane:Methanol 10:1). The yield: 0.29 g (81%), m.p. 115 °C (Scheme 1). UV–vis: λ_{max} 294, 362 nm. FT-IR: 3300 cm^{-1} (ν_{OH}), 3020 cm^{-1} (ν_{NH}), 1624 cm^{-1} ($\nu_{C=N}$ of imine), 1589 cm^{-1} ($\nu_{C=N}$ of imidazole). ^1H NMR (400 MHz, DMSO-d_6, 25 °C): δ = 12.62 (s, 1H), 9.78 (s, 1H), 7.80, 7.72 (dd, 2H), 7.26 (s, 1H), 6.84, 6.75 (d, 1H), 6.51, 6.49 (d, 1H), 2.50 (s, 3H) ppm. ^{13}C NMR (400 MHz, DMSO-d_6, 25 °C); δ = 162.88, 148.20, 138.25, 136.46, 131.80, 128.38, 124.51, 122.48, 122.10, 117.81, 20.98 ppm. LC–MS: m/z calcd for $C_{11}H_{11}N_3O$—H^+: 200.40; found 200.04. CHN analysis calcd

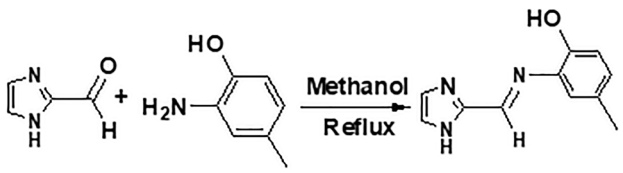

Scheme 1 Synthesis of IMP

(%) for $C_{11}H_{11}N_3O$ (201.09): C, 64.98; H, 5.01; N, 21.23; O, 7.35; found: C, 64.78; H, 5 0.12; N, 20.98; O, 7.15.

Analytical Procedure

Fluorescence Titration of IMP with Zn^{2+}

Probe IMP (96 mg, 1 mmol) was dissolved in 1:9, v/v 0.01 M H_2O-DMF, pH 7 (5 ml). $Zn(OAc)_2{\cdot}H_2O$ (1 mmol) was dissolved in 1:9, v/v 0.01 M H_2O-DMF, pH 7 (5 mL). Taking 2 mL from each solution and mixing them for a few seconds, fluorescence spectra were taken at room temperature.

UV–visible Titration of IMP with Zn^{2+}

Probe IMP (96 mg, 1 mmol) and $Zn(OAc)_2{\cdot}H_2O$ (1 mmol) were dissolved in DMF solution (5 mL). 0.5–5 µL of the prepared solution was carried for took UV–vis absorption spectra at room temperature.

Job's Plot Measurement of Zn^{2+}

Probe IMP (1 mmol) was dissolved in 1:9, v/v 0.01 M H_2O-DMF, pH 7 (5 mL).Prepared$Zn(OAc)_2{\cdot}H_2O$ (1 mmol) solution in 1:9, v/v 0.01 M H_2O-DMF, pH 7 (5 mL). 30–170 µL of the analyte solutions were taken and added probe solutions were until it contains 200 µL in each vial. Each vial was then diluted with DMF to make a total volume of 3 mL. Shaken well the solutions for a few minutes, fluorescence spectra were taken at room temperature.

Detection of Zn^{2+} with IMP—Competition Experiment.

Stock solutions for various metal ions (Cu^{2+}, Fe^{2+}, Fe^{3+}, Ni^{2+}, Co^{2+}, Mg^{2+}, Zn^{2+}, Cd^{2+}, Na^{+}, K^{+}, In^{3+}, Sr^{2+}, Mn^{2+}, Hg^{2+} and Pb^{2+} were prepared with a 1.0×10^{-3} M concentration using metal anions in deionized water, and the pH was 6.45. The solution of the probe IMP was prepared with a concentration of 1.0×10^{-3} M in DMF, and the pH of the solution was nearly 7.

Quantum Yield Measurement

Quantum yield (QY) is defined as the efficiency of converting absorbed light into emitted light, which can be in the form of fluorescence. The QY of IMP and IMP-Zn^{2+} was measured by a comparative fluorescence method using Rhodamine B in 1×10^{-3} M DMF as the standard (std) solution (QYstd = 0.97 at an excitation wavelength of 414 nm, nstd = 1.36). The QY of probe and complex were calculated by Eq. (1).

$$QYSample = QYreference \times \frac{ms}{mr} \times \left[\frac{\eta s}{\eta r}\right]2 \quad (1)$$

Where ms, mr, ηs, and ηr represent slope and refractive index of the solvent of sample and reference which is measured by fluorescence spectrophotometer, respectively.

Calculation of the Binding Association Constant for IMP-Zn^{2+} Complex

The association constant (K_a) was calculated using the Benesi-Hildebrand plot (or a double-reciprocal plot) as shown in Eq. (2).

$$\frac{1}{I-I0} = \frac{1}{Ka}x(Imax-I0)x[Zn2+] + \frac{1}{Imax-I0} \quad (2)$$

where; I is the experimentally measured fluorescence intensity, I0 is the fluorescence intensity of probe IMP alone, and Imax is the saturated fluorescence intensity of the IMP- Zn^{2+} complex.

Quantification of Zn^{2+} in Real Samples

The application study of probe IMP has been done in two different kinds of water samples collected from our home. The fluorescent analysis was carried out by adding 50 µL (1 mmol) of probe IMP to a 3 mL real sample solution having Zn^{2+}. Solutions were blended for about 10 min at 25 °C. Their fluorescence spectra were obtained.

Colorimetric Chemosensor

Naked Eye and UV–vis Detection of Co^{2+}

Receptor IMP (96 mg, 1 mmol) was dissolved in a set of polar and non-polar solvents (2 mL) and 20 µL of the receptor IMP was mixed with 20 µL of $Co(OAc)_2{\cdot}H_2O$ solution in DMF. After few seconds, UV–visible absorption spectra were taken at room temperature.

Job's Plot Measurement of Co^{2+}

Receptor IMP (96 mg, 1 mmol) was dissolved in DMF (2 mL). Added 30–170 µL of the analyte solutions into receptor solutions taken in each cuvet by made up to a total of 200 µL volume. DMF was poured to mark up to 3 mL volume of the total solution. After shaking the solutions, UV–visible absorption spectra were recorded at room temperature.

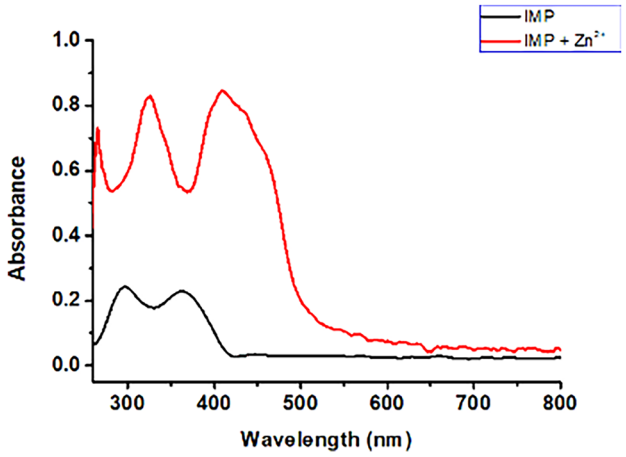

Fig. 1 A comparative UV–visible spectra of IMP and IMP-Zn^{2+}

Detection of Co^{2+} with IMP—Competition Experiment.

For the color change analysis, UV–visible spectra were recorded. The colorimetric detection of various metal ions was carried out at room temperature using 1 mL volume of each metal ion solution of a 1.0×10^{-3} M concentration and 1 mL of the Schiff base ligand (1.0×10^{-3} M), and the solution mixture was diluted to 10 mL by adding the DMF solvent. The pH of the solution mixture was 7.25. After mixing properly, the UV–visible spectra of the mixtures were recorded.

Calculation of the binding association constant for IMP-Co^{2+} complex

The association constant (K_a) was calculated using the Benesi-Hildebrand plot (or a double-reciprocal plot) as shown in Eq. (3).

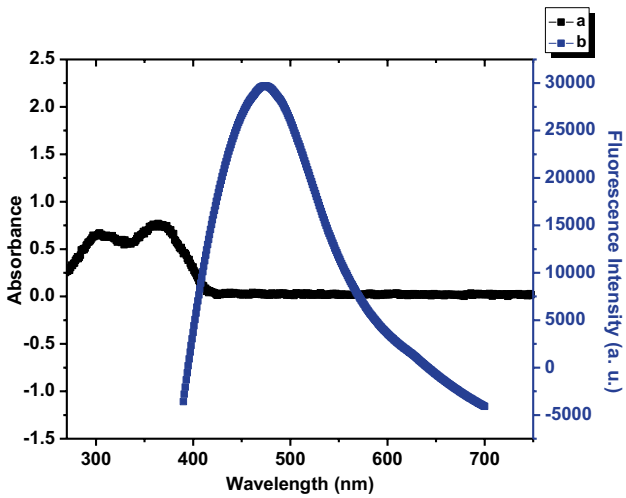

Fig. 2 Combined spectra of IMP, **a** UV–visible spectrum of IMP, **b** Fluorescence spectrum of IMP

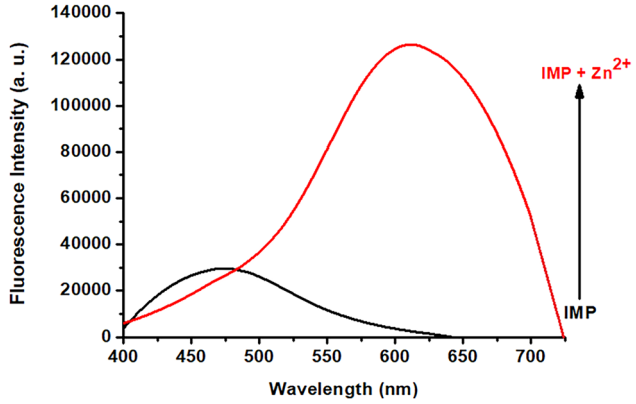

Fig. 3 Combined fluorescence spectra of ligand IMP and IMP + Zn^{2+}

$$\frac{1}{A-A0}=\frac{1}{Ka}x(Amax-A0)x[Co2+]+\frac{1}{Amax-A0} \quad (3)$$

Where; A is the experimentally measured absorbance intensity, A0 is the absorbance intensity of probe IMP alone, and Amax is the saturated absorbance intensity of the IMP- Co^{2+} complex.

Results and Discussion

We synthesized the new imidazole bound system as a sensor molecule IMP by following the general route of bonding a hetero aromatic aldehyde to an aromatic cresol and characterized by CHN analysis, UV–visible, FT-IR, elemental analysis, LC–MS and ^{1}H and ^{13}C NMR techniques.

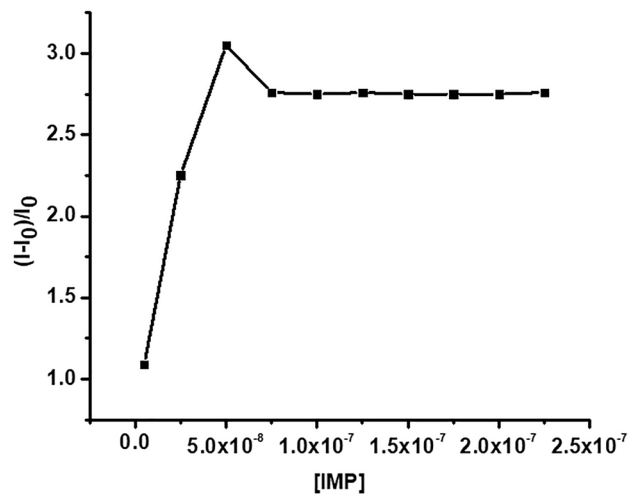

Fig. 4 Effect of concentration of IMP on fluorescence change of the system

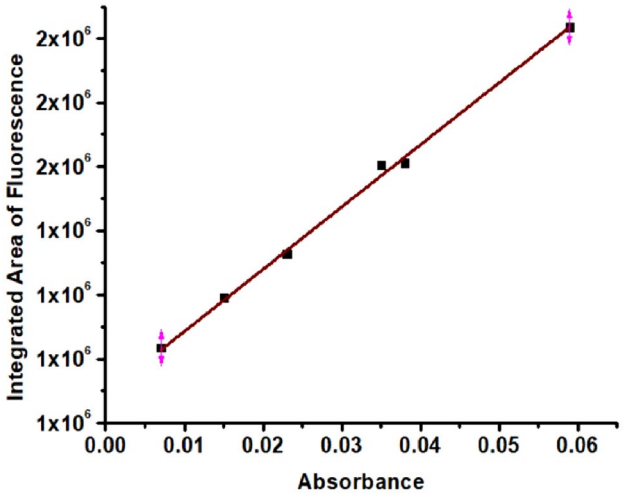

Fig. 5 QY graph of ligand IMP

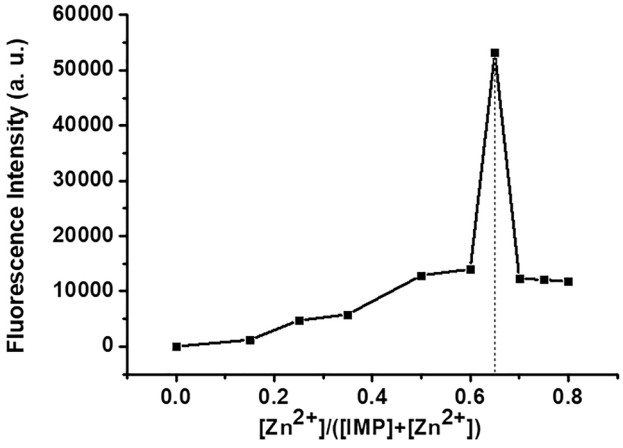

Fig. 7 Job's plot of IMP and Zn^{2+}

Spectral Characterizations

The elemental concentrations of carbon, hydrogen, and nitrogen in the synthesized ligand were determined using CHN analysis. The results indicate that the synthesized compound is analytically pure and is in good agreement with the proposed chemical formula. The electronic spectral investigations were carried out in 1.0×10^{-5} M DMF solution of ligand in the range of 200–800 nm. The spectral assignments for electronic transitions in ligand and peaks attributed to starting materials lying in the region of 200–260 nm and 200–300 nm for aldehyde and amine respectively. As per the spectra, a new peak is formed in the region of 350–370 nm indicated the presence of the imine group. The two absorption maxima corresponding to two intra ligand transitions: a weak peak and a strong peak at 294 nm and 362 nm. Low energy band is due to $n \rightarrow \pi^*$ on -HC = N- group which is characteristic of the Schiff base [31]. The high energy band can be attributed to the $\pi \rightarrow \pi^*$ transitions on imidazole and phenol aromatic rings [32]. The important bands observed in the IR spectrum of the ligand along with their functional group assignments as per the literature data of similar compounds and the four characteristic peaks around 3300 cm^{-1}, 3020 cm^{-1}, 1624 $cm^{-1}$and 1589 cm^{-1} were registered as vibrational modes of O–H stretching, N–H stretching, C = N of newly formed imine and C = N of aromatic imidazole ring [33, 34]. Mass spectrometry was performed on the IMP ligand to determine its molecular weight and fragmentation pattern. The molecular ion peak $[M\text{-}1]^+$ was observed at m/e 200.4, confirming the formula weight (F.W.) which is the same as the calculated M^+ value. ^{1}H NMR and ^{13}C NMR spectrum of the IMP indicated the proof for ligand formation. Singlet in the region of 2.50 ppm is due to the presence

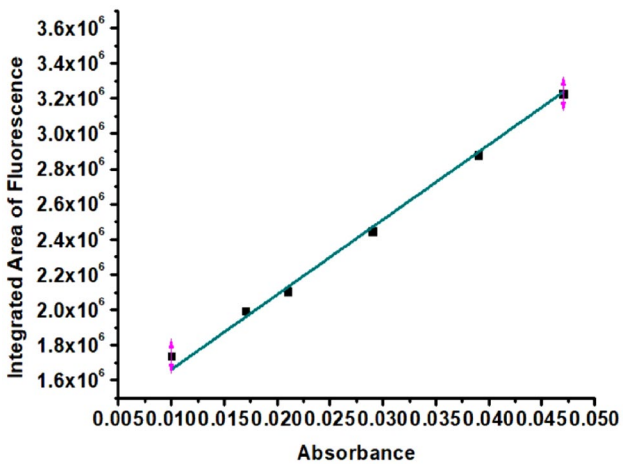

Fig. 6 QY graph of IMP + Zn^{2+}

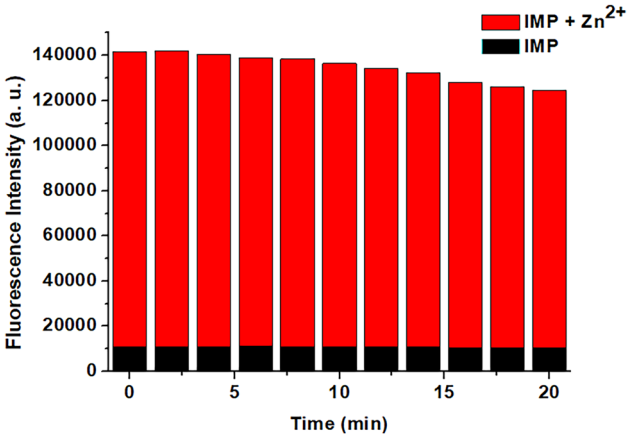

Fig. 8 Effect of time on IMP and IMP-Zn^{2+}

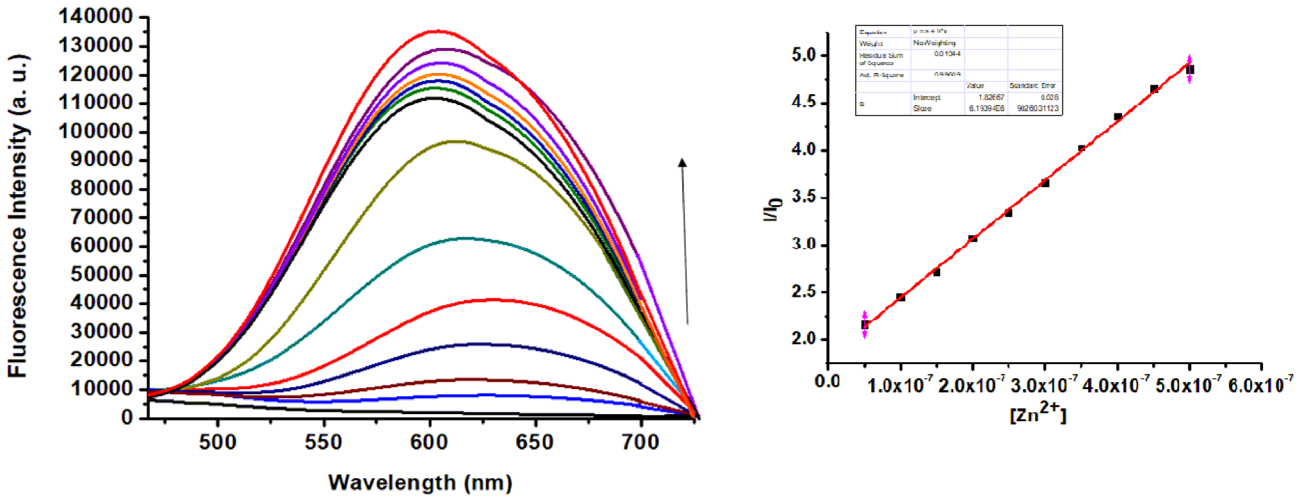

Fig. 9 Effect of concentration of Zn^{2+} on the fluorescence intensity of IMP and inset represents linear calibration graph between the ratio of fluorescence intensities and concentrations of Zn^{2+}

of methyl protons. The presence of singlet at 9.78 ppm is caused due to the presence of imine H. Another downfield singlet discernible at around δ 12.63 was allotted to NH proton. The fairly higher downfield effect on NH proton owed to strong intramolecular H bonding. The remaining protons of aromatic moieties were present in the form of singlet and doublets at δ 6.49–7.80 ppm [35]. The proton decoupled ^{13}C NMR spectrum provides direct information about the carbon skeleton of the molecule. Signals around 122 and 136 ppm corresponds to carbons of the imidazole ring. Aromatic carbons of phenol ring resonate between 117–140 ppm. A high value near 162 ppm is due to the presence of imine carbon. Carbon attached to OH resonates at 148 ppm. The methyl group in phenol resonates at 20 ppm [36].

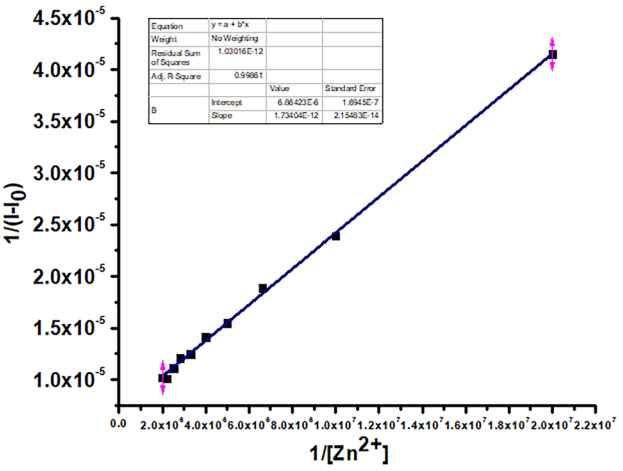

Fig. 10 Linear representation of binding constant for IMP-Zn^{2+} complex

Optical Response of IMP Towards Zn^{2+}

The ligand IMP contains imidazole moiety is frequently found as an indispensable piece of a fluorophore which gives oxygen to metal coordination and an acidic proton which could be lost open metal chelation to frame a monoanionic compound. Also, the lone pairs on imine nitrogen and solitary sets on imidazole nitrogen have been adding to develop a steady metal complex by clung to the empty d orbital of metals. The underlying visibility and substance properties are anticipated to prompt metal particle holding qualities not quite the same as the noticed for the beginning materials. Then, we inspected the UV–visible titration for IMP by adding traces of Zn^{2+} metal solution in DMF. At the point when the sensor IMP was titrated with Zn^{2+}, there seen a bathochromic shift in the frequency range, 410–430 nm with higher absorption maxima even at lower concentrations of

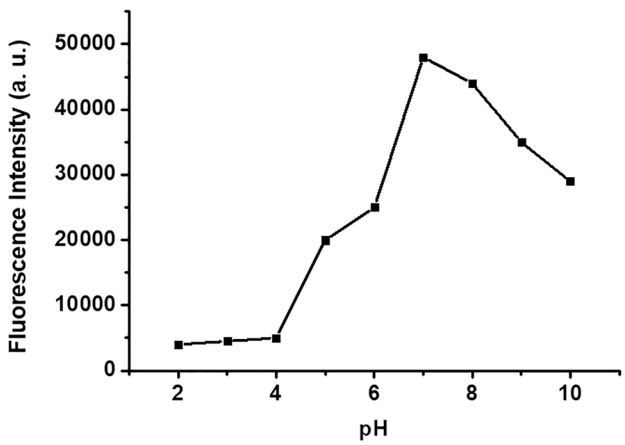

Fig. 11 Effect of pH on IMP

Scheme 2 Proposed binding mechanism of IMP with Zn^{2+}

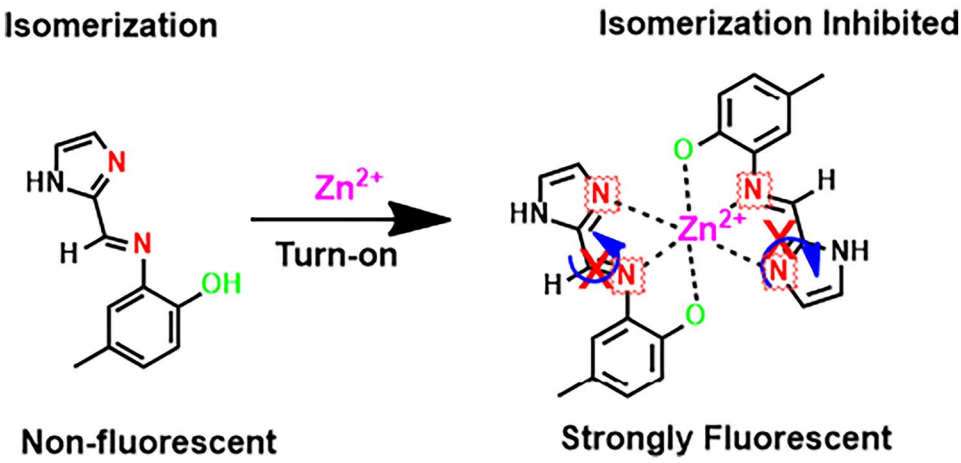

the analyte. Additionally, the peaks at 294 nm and 364 nm for the IMP ligand were dense together to form a new peak in the area of 340–350 nm for the metal complex (Fig. 1). The new peak formed thus confirmed the clean conversion of IMP to IMP-Zn^{2+} complex.

The photophysical properties and sensing behavior of the ligand IMP were investigated using UV absorption and fluorescence spectroscopy. First, the UV–vis spectrum of the ligand IMP (1×10^{-3} M) was recorded in DMF. IMP exhibited two absorbance peaks at 294 and 364 nm corresponding to the $\pi - \pi^*$ and $n - \pi^*$ transitions, respectively. Also, the fluorescence emission spectra of IMP were measured in DMF (1×10^{-3} M) and the emission peak was observed at 474 nm for IMP. The ligand exhibited excellent absorption and fluorescent characteristics are shown in Fig. 2.

Upon the addition of Zn^{2+} ions to IMP in DMF, attractive change has been noticed (Fig. 3), where the fluorescent intensity peaks for ligand would disappear and a new peak with enormous fluorescent enhancement is observed at 612 nm. Since the ligand is non-fluorescent showed a fluorescent intensive peak around the region 474 nm. The complete disappearance of peak obtained for IMP alone in IMP-Zn^{2+} complex confirmed the chelation power of metal towards the active site of the ligand.

We have investigated the concentration of ligand IMP to attain sensitivity. A graph was plotted on the concentration of IMP with a difference in fluorescence intensity, $(I\text{-}I_0)/I_0$, where I_0 is the fluorescence intensity of probe alone and I is the fluorescence intensity of probe with an analyte. In Fig. 4, there was a sharp increase in intensity on increasing

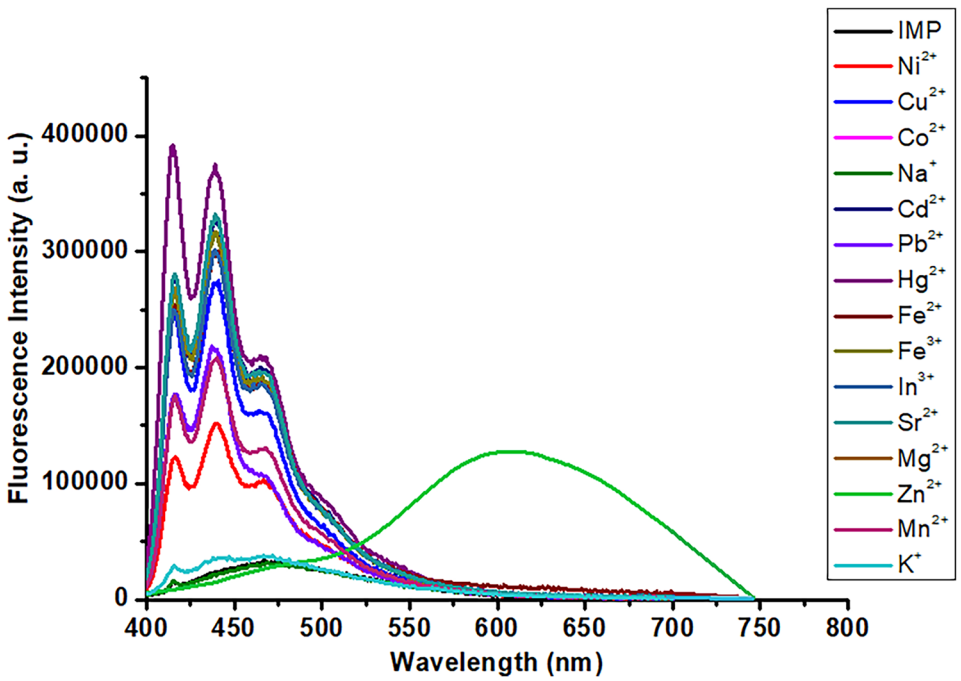

Fig. 12 Fluorescent intensity of IMP in DMF due to 1 equi. of metal ion. The fluorescence due to Zn^{2+} is shown as a new peak and fluorescence due to other metal ions and IMP are the baseline curves

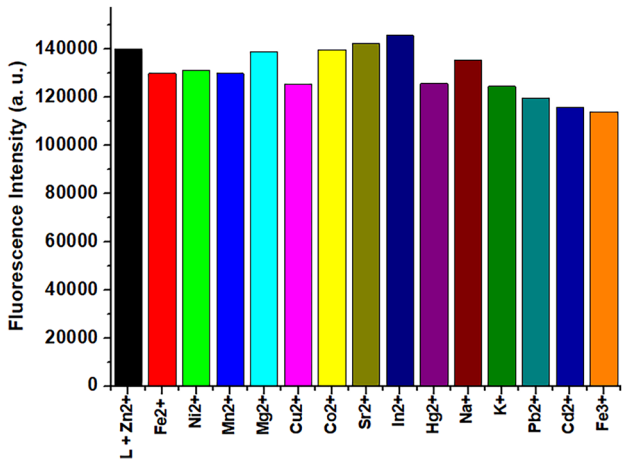

Fig. 13 Interference fluorescence of IMP-Zn^{2+} complex in the presence of various metal ions

the concentration of probe but reached a maximum value at 5×10^{-8} M and becomes constant. Hence we used the same for further studies.

The QY graphs are plotted against absorbance versus fluorescence intensity for IMP alone (Fig. 5) and IMP-Zn^{2+} (Fig. 6). From the QY calculations (Eq. 1), the fluorescence quantum yields of probe IMP in the free and Zn^{2+} bound state were found to be 0.0093 and 0.7873 respectively. However, probe with Zn^{2+} with quantum yields higher than 0.1 is still considered quite fluorescent and IMP with quantum yield lesser than 0.1 is considered as non-fluorescent [37].

A job's plot was drawn by taking the concentration of analytes on x-axis and fluorescence intensity corresponds to the analyte in y-axis showed the 1:2 binding between analyte Zn^{2+} and the probe IMP (Fig. 7). Further characterization of IMP-Zn^{2+} complex was done by CHN analysis. calcd (%): C, 57.89; H, 5.67; N, 16.88; O, 6.43. This might be a piece of evidence for the 1:2 molar complexation of the probe with an analyte.

Change in fluorescence intensity with time was studied by illuminating the probe solution in the absence and presence of Zn^{2+} respectively. The IMP solution gave a stable fluorescence signal up to 21 min. Upon addition of Zn^{2+}, the fluorescence intensity of the probe enhanced with much more photostability which eliminates the time -consuming incubation step disposes by many of the existing methods for real samples (Fig. 8).

Execution of the Sensor

Effect of Concentration

On expanding the centralization of Zn^{2+}, a consistent expansion in the intensity just as an adjustment of the shape of the fluorescence signal was noticed (Fig. 9). A calibration graph was plotted with a concentration of Zn^{2+} against I/I_0, and it was found to be linear in the range 5×10^{-8} to 5×10^{-7} M (inset of Fig. 9). The limit of detection and limit of quantification was calculated using equations '3S/ m' and '10S/ m', where 'S' was the standard deviation and 'm' was the slope of the calibration graph. The limit of detection and limit of quantification was found to be 6.78×10^{-9} M and 2.26×10^{-8} M respectively. In the presence of Zn^{2+}, the probe IMP shows selective chelation enhanced fluorescence (CHEF) [38, 39]. The upgrade in fluorescence spectra in this manner force inflexibility and consequently decline the nonradiative decay of the energized state. In out range focus, the intensity of IMP isn't change due to the zinc particle uncomplexed.

The binding association constant (K_a) was graphically evaluated by plotting $1/(I-I_0)$ versus $1/[Zn^{2+}]$, as shown in Fig. 10. From the linear relationship graph, the K_a value calculated from Eq. (2) was 3.96×10^6 M^{-1}.

Table 1 Comparison of the characteristics of the IMP sensor with those of the previously reported Zn^{2+} sensor

Sensor	Dynamic Range (M)	Detection Limit (M)	Interfering Ions	Ref
4-chloro-2-(5-phenyl-1-(pyridin-2-yl)-4,5-dihydro-1H-pyrazol-3-yl)phenol	0 to 7.0×10^{-6}	1.2×10^{-7}	Ni^{2+}, Cd^{2+}, Co^{2+}, Cu^{2+}	[38]
Tris(3-(2-hydroxyacetophenone)propyl)amine	1.6×10^{-7} to 5.0×10^{-5}	8.8×10^{-8}	Cu^{2+}	[41]
(E)-3-((4-(diethylamino)-2-hydroxybenylidene)amino)-2,3-dihydrothiophene-2-carboxamide	0 to 8×10^{-5}	2.55×10^{-6}	No interference	[42]
2-[(2-Hydroxy-benzyl)-pyridin-2-ylmethyl-amino]-N-quinolin-8-yl-acetamide	-	66×10^{-9}	Ni^{2+}, Fe^{2+}, Co^{2+}, Cu^{2+}	[37]
N,N phenylenebis salicylideaminato	1.6×10^{-7} to 1.0×10^{-5}	1.5×10^{-7}	Co^{2+}	[43]
(E)-(2-((2-nitrobenzyl)(2-((E)-(2-hydroxynaphthalen-1-yl)methyleneamino)ethyl)amino)ethylimino)methyl) naphthalen-2-ol	-	1.0×10^{-7}	-	[39]
2-[(1H-imidazole-2-ylmethylene)-amino]-4-methyl-phenol	5×10^{-8} to 5×10^{-7}	6.78×10^{-9}	No interference	This work

Fig. 14 Color of IMP upon addition of various metal ions

Effect of pH

To find out whether the probe IMP is stable at acidic or basic pH conditions, we need to take the fluorescence spectra in the pH range 1–10 (Fig. 11). From which, we have remarked that the highest fluorescent intensity was observed at pH 7 indicated the stability of probe in basis buffer. Hence, we did further experiments in the same buffer solution.

Mechanism of Zn^{2+} Detection

The probe, IMP alone could act as a non-fluorescent system and becomes highly fluorescent upon binding with Zn^{2+} ions due to the formation of a rigid system. We have been attempted to be rationalized on the basis of PET mechanism, which is a commonly used strategy for metal sensing fluorosensors showing intensity enhancement in the presence of suitable metal ions. The enhanced fluorescence in our system is a consequence of combined effects of chelation-enhanced fluorescence (CHEF), C = N isomerization, and inhibition of photo-induced electron transfer (PET). In order to substantiate it, the quantum yield values for IMP before and after binding have been undertaken [40].Scheme 2 Proposed binding mechanism of IMP with Zn2+Scheme 2 Proposed binding mechanism of IMP with Zn2+Scheme 2 Proposed binding mechanism of IMP with Zn2+

Selectivity and Interference Studies

Perhaps the main property of a sensor are its selectivity. To contemplate the selectivity of the test, various species (1×10^{-5} M) that are either primarily comparable or coinciding or the same grouped metal ions were taken and their effect on fluorescence intensity of IMP was noticed. The fluorescent enhancement in the spectra is not seen for other metal ions such as Cu^{2+}, Fe^{2+}, Fe^{3+}, Ni^{2+}, Co^{2+}, Mg^{2+}, Cd^{2+}, Na^{+}, K^{+}, In^{3+}, Sr^{2+}, Mn^{2+}, Hg^{2+}, and Pb^{2+}. The selectivity of the probe towards Zn^{2+} is shown in Fig. 12. Hence the sensor should be an ideal probe for zinc-containing samples while the sample has metals of a similar group. Noting the selective fluorescence enhancement due to Zn^{2+}, metal ions were tested for their ability to inhibit the fluorescence of the IMP-Zn^{2+} complex. The metal ions selected for interference studies were Cu^{2+}, Fe^{2+}, Fe^{3+}, Ni^{2+}, Co^{2+}, Mg^{2+}, Cd^{2+}, Na^{+}, K^{+}, In^{3+}, Sr^{2+}, Mn^{2+}, Hg^{2+}, and Pb^{2+}. The intensity of the peak of IMP with Zn^{2+} had no effect upon addition with metal ions except for Fe^{3+}, Hg^{2+}, Cu^{2+}, and Cd^{2+} (Fig. 13). The later metal ions might interfere with the peak intensity with a signal change of 5%. Meanwhile, upon adding more equivalents of metal ions (1:5, 1:10, etc.), the fluorescent intensity peaks get lowered with significant interference.

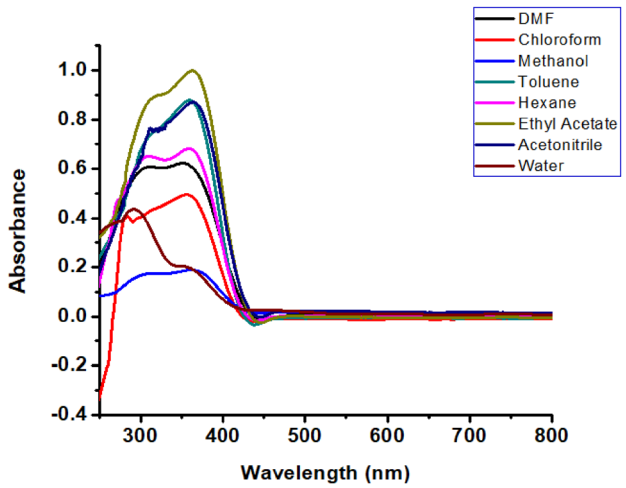

Fig. 15 UV–visible spectrum of IMP in various solvents

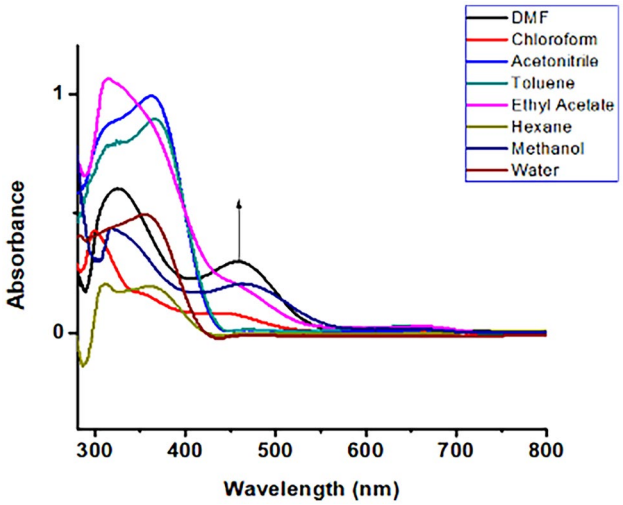

Fig. 16 UV–visible spectrum of IMP-Co^{2+} in various solvents

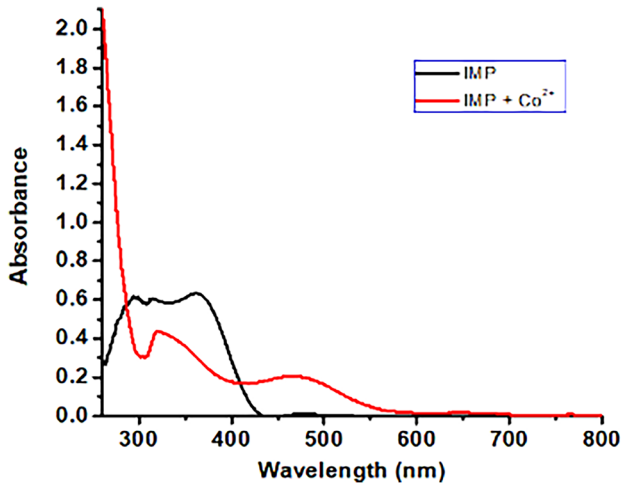

Fig. 17 A comparative UV–visible spectra of IMP and IMP + Co^{2+}

It was found that the probe IMP exhibits an off–on-type mode with high selectivity in the presence of Zn^{2+} ions. The fluorescence spectra results revealed that the fluorescence emission intensity of probe IMP decreased dramatically on complex formation and the Zn^{2+} complexes showed high emission maxima. In addition, the examination of the characteristics of the IMP sensor with those of the recently announced Zn^{2+} sensor is organized in Table 1.

Colorimetric Chemosensor

During the fluorescence investigation of detecting Zn^{2+} in DMF, we noticed the color changes of IMP within the sight of Co^{2+} ion instead of some other metals. Consequently, we inspected the chromogenic detecting capacity of IMP within

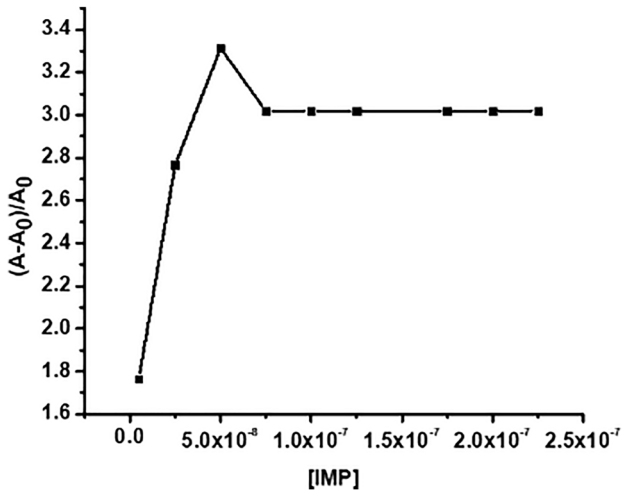

Fig. 18 Effect of concentration of IMP on absorbance change of the system

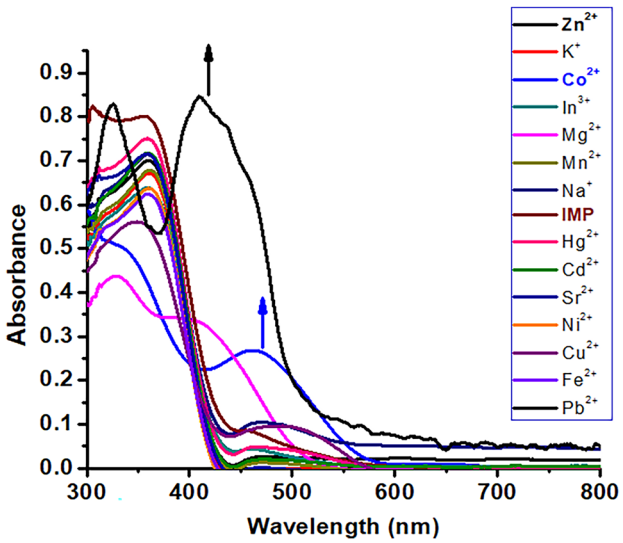

Fig. 19 UV–visible absorption spectra of IMP in the presence of different metal ions (1:1)

the sight of an assortment of metal particles like Cu^{2+}, Fe^{2+}, Ni^{2+}, Co^{2+}, Mg^{2+}, Zn^{2+}, Cd^{2+}, Na^{+}, K^{+}, In^{3+}, Sr^{2+}, Mn^{2+}, Hg^{2+}, and Pb^{2+} in DMF. The receptor IMP showed prompt color changes from dull to pink in the presence of Co^{2+} and a very low yellow intense in presence of Zn^{2+} which was purposefully omitted. While different metals caused no adjustment of color (Fig. 14).

However, the receptor IMP was miscible completely in DMF and other organic solvents. Even there seen partial miscibility in presence of highly polar water solvent with low-intensity peak assigned for $n \rightarrow \pi^*$ transition which was inferred from the UV–visible spectrum (Fig. 15). All other

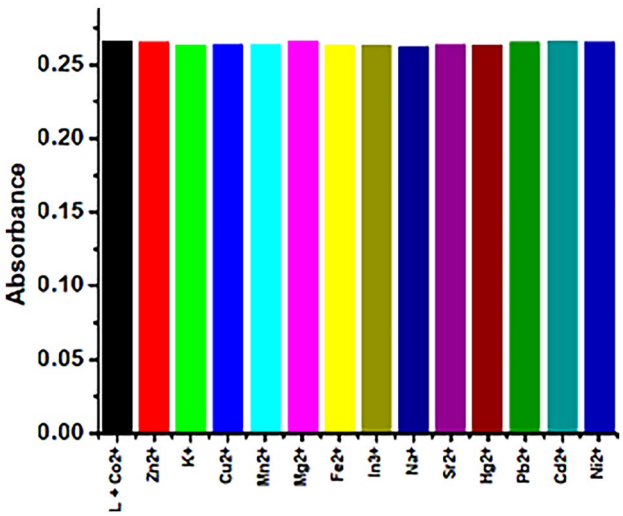

Fig. 20 UV–visible absorption spectra of IMP-Co^{2+} in the presence of different metal ions (1:1)

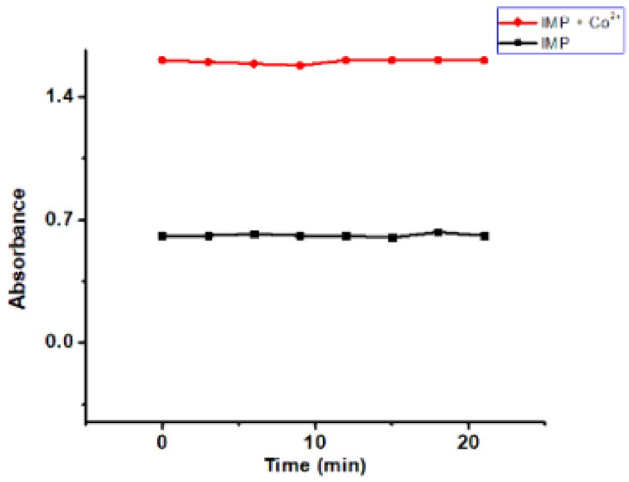

Fig. 21 Relative effect of time on IMP and IMP-Co^{2+}

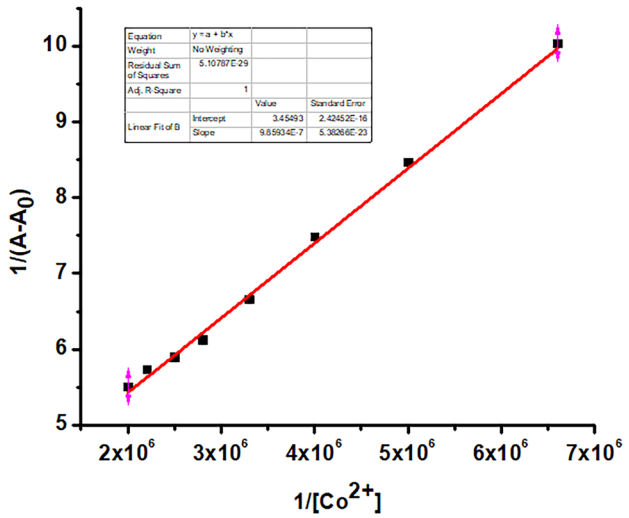

Fig. 23 Linear representation of binding constant for IMP-Co^{2+} complex

solvents do not cause any change in the absorption spectrum of IMP since it has two peaks in the region of 312 nm and 358 nm as weak and strong peaks respectively. So the need for solvent effect in the UV–visible spectra of IMP with $Co^{2+}$is mandatory. Upon adding Co^{2+}, a new peak was formed at 474 nm indicated the transfer of free ligand into the metal complex. Even though, DMF is the best solvent for the complexation of receptor IMP with Co^{2+} ion with an enhancement in the absorption intensity at 460 nm was cleared from Fig. 16. Hence we continued the studies in DMF and not with buffer solutions. The UV–visible spectra changes of IMP and IMP-Co^{2+} was shown in Fig. 17.

The sensitivity of receptor IMP towards Co^{2+} was determined. The concentration of receptor IMP was obtained by plotting [IMP] against $(A\text{-}A_0)/A_0$ (Fig. 18) and it was found to be 5×10^{-8} M where A_0 is 0.051 nm. The selectivity of receptor IMP towards various metal ions (Fig. 19) suggested the future scope of the sensor with rapid determination and efficacy. No other metals shown any color change and characteristic peak in the region of 450–475 nm. The new peaks formed in the IMP-Co^{2+} complex might be attributed to metal to ligand charge transfer (MLCT), which is responsible for the pink color of the solution. Moreover, it is qualified to specify that the receptor IMP could be utilized as a test for the separation of Co^{2+} from Zn^{2+} by the naked eye.

To examine the interference of IMP-Co^{2+} complex in presence of other competing metal ions such as like Cu^{2+}, Fe^{2+}, Ni^{2+}, Mg^{2+}, Zn^{2+}, Cd^{2+}, Na^{+}, K^{+}, In^{3+}, Sr^{2+}, Mn^{2+},

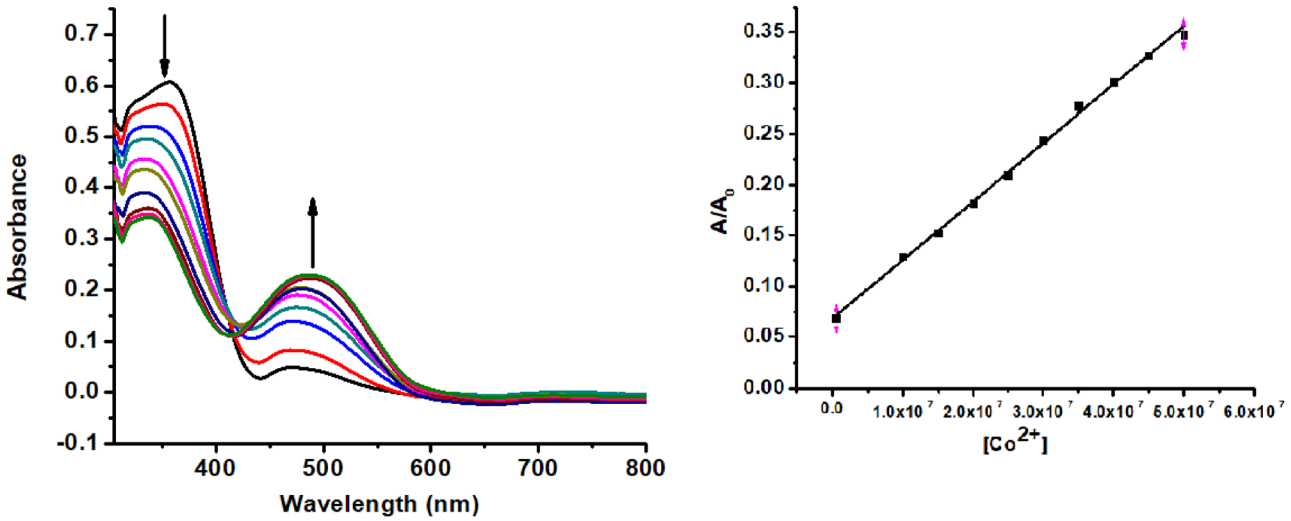

Fig. 22 Effect of concentration of Co^{2+} on the UV–visible absorption spectra of IMP. 10 to 100 µL of (10^{-5} M) Co^{2+} solutions were added to receptor IMP and inset represents linear calibration graph between the ratio of UV–visible absorptions and concentrations of Co^{2+}

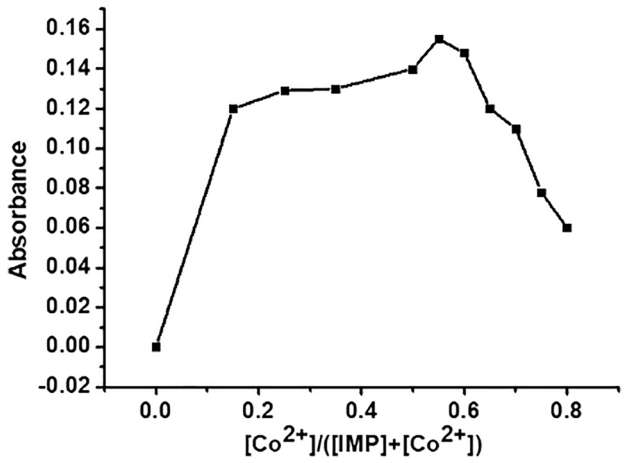

Fig. 24 Job's plot of IMP and Co^{2+} in DMF. Total concentrations of IMP and Co^{2+} were 200 µL

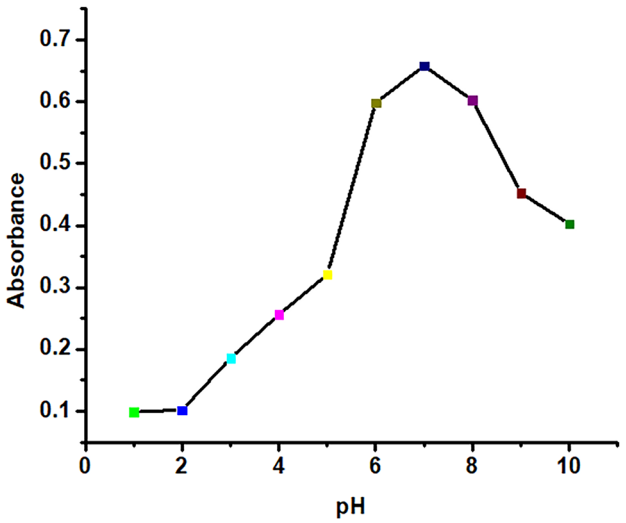

Fig. 25 Effect of pH of IMP on absorbance spectra

Hg^{2+}, and Pb^{2+}, the UV–visible competitive studies were graphically implemented (Fig. 20). Background of most competing metal ions did not interfere with the naked-eye detection of Co^{2+} even in one equivalences (1:1) and multiple equivalence (1:10 and 1:50) of other metal ion solutions.

Next, we need to investigate the time stability of receptor IMP alone and IMP-Co^{2+} complex in a period of 0–21 min at room temperature (Fig. 21). From the spectra, there should be no change in the characteristic peaks for IMP and IMP-Co^{2+} as time consumes. Thus it was kept for a long period of time without any reduction in the intensity of spectra, which will lead to the application studies in biological samples in future.

On comparing the incorporation of Co^{2+}, a gradual expansion in the intensity of absorption spectra with some sort of the change in the peaks maxima was identified (Fig. 22). A linear calibration graph was plotted with a concentration of Co^{2+} against A/A_0, where A & A_0 are the absorptions of analyte and probe respectively. It was found to be linear in the range 5×10^{-8} to 5×10^{-7} M (inset of Fig. 22). The limit of detection and limit of quantification was found to be 6.74×10^{-9} M and 2.22×10^{-8} M respectively. Imidazole bound sensor system is still unaware for the researchers and our proposed sensor with better detection limit value would definitely detect the Co^{2+} at the commercial level.

The binding association constant (K_a) for IMP-Co^{2+} was graphically evaluated by plotting $1/(A-A_0)$ versus $1/[Co^{2+}]$, as shown in Fig. 23. From the linear relationship graph, the K_a value calculated from Eq. (3) was 3.50×10^6 M^{-1}.

Stoichiometry of the IMP-Co^{2+} complex was determined by Job's plot which revealed 1:2 ratio (Fig. 24) might be in good agreement with the analyte Zn^{2+} discussed above. There is a smooth transformation of receptor IMP into the cobalt complex by effective binding with possible donor atoms in the IMP or supported by the PET mechanism. In short, the comparison of IMP and other reported sensors with analyte Co^{2+} is presented in Table 2.

We took the absorbance spectra of receptor IMP at various pH conditions (Fig. 25). It is highly stable at alkaline pH conditions and thus, we did further experiments in the same buffer condition.

Table 2 Comparison of the characteristics of the IMP sensor with those of the previously reported Co^{2+} sensor

Sensor	Dynamic Range (M)	Detection Limit (M)	Ref
2,6-bis(iminomethyl)pyridine	5×10^{-4} to 5×10^{-3}	-	[44]
DISN	0 to 10×10^{-6}	1.24×10^{-7}	[45]
BNHNTA	0.1 to 1.2×10^{-6}	0.05×10^{-6}	[46]
Methylene blue, Aminothiophenol and Copper nitrate complex	-	0.04×10^{-3}	[47]
2,2′:6′,2″-terpyridine and 2,2′-dihydroxyazobenzene	-	0.45×10^{-6}	[48]
2-Chloro-N-(quinolin-8-yl) acetamide and 2-(((pyridin-2-yl) methylamino) methyl)phenol	-	0.85×10^{-6}	[49, 50]
IMP	5×10^{-8} to 5×10^{-7}	6.74×10^{-9}	This work

Table 3 Determination of Zn^{2+} ion in water samples with probe IMP

Sample	Zn^{2+} Added (μmol/L)	Zn^{2+} Found (μmol/L)	Recovery (%)	R.S.D (n = 3) (%)
Drinking Water	15	14.2 ± 0.4	97.3 ± 1.0	4.01 ± 0.8
Tap Water	15	14.8 ± 0.6	98.5 ± 1.2	1.21 ± 1.3

*Results are based on three measurements

Analytical Application of Detection of Zn^{2+} in Water Samples

To get clear knowledge on the selectivity conduct, its higher selectivity for zinc discovery in this technique, displayed by the mentioned sensor, makes it fantastic for observing zinc particles at following fixations in various water samples. Drinking water and tap water were taken and diluted with a buffered solution in a 25.0 mL volumetric flask. Various measures of Zn^{2+} ions were added to water tests. The proposed sensor was utilized in request to decide the Zn^{2+} content thus the calibration technique was applied. The results obtained with the sensor are mentioned in Table 3. It was also found that the accuracy of Zn^{2+} detection in different water samples gives out way to biological sample quantification [41].

Conclusion

A new versatile, simple, selective, and efficient imidazole bound Schiff base has been synthesized and characterized. It exhibited a remarkable selectivity and sensitivity towards Zn^{2+} by fluorescence spectra and for Co^{2+} by UV–visible spectra over competing for other relevant metal ions. The detection limit of the probe with Zn^{2+} and Co^{2+} are far below as compared with other reported sensors. The binding ratios of the probe to M^{2+} ($M^{2+} = Zn^{2+}$, Co^{2+}) are 2:1 and the metal association constants are in the 10^6 M^{-1} range. The probe binds to Zn^{2+} through four nitrogen atoms and does so through the phenolic oxygen. Thus the results reported here provide a novel approach for the simultaneous selective identification of Zn^{2+} and Co^{2+} among various metal ions. The attractive properties of this method such as selectivity and rapidness would help us to extend its applications for the determination of Zn^{2+} ions in water samples.

Supplementary Information The online version contains supplementary material available at https://doi.org/10.1007/s10895-021-02839-5.

Acknowledgements The authors would like to express their gratitude to CUSAT, Kerala, India for financial assistance and STIC, CUSAT for the real time analyses.

Authors' contributions Anjali Krishna Gopalakrishnan has written the manuscript and all the data's were interpreted according with the obtained results. Shanty Antony Angamaly helped in the interpretation of mechanism of detection. Savitha Devaswamparambil Pradeep helped in doing application studies. Dhanya Thaikatt Madhusudhanan contributed in fluorescence studies. Divya Kizhakkeppurath Manoharan contributed in analyzing data. Puzhavoorparambil Velayudhan Mohanan helped in interpretation of data.

Funding NA.

Data Availability All data analysed in this study are included in this article. If more supporting information is needed it can be available on request from the corresponding author (Mohanan P.V.).

Code Availability NA.

Declarations

Ethics Approval NA.

Consent to Participate NA.

Consent for Publication NA.

Conflict of Interest The authors declare that they have no conflict of interest.

References

1. Gale P, Caltagirone C (2018) Coord Chem Rev 354:2–27
2. Kaur B, Kaur N, Kumar S (2018) Coord Chem Rev 358:13–69
3. Upadhyay S, Singh A, Sinha R, Omer S, Negi K (2019) J Mol Struct 1193:89–102
4. Liu Q, Liu T, Fang Y (2020) Langmuir 36:2155–2169
5. Luo X, Han Y, Chen X, Tang W, Yue T, Li Z (2020) Trends Food Sci Tech 95:149–161
6. Shamsipur M, Barati A, Nematifar ZJ (2019) Photochem Photobiol Rev 39:76–141
7. Antony R, Arun T, David Manickam S (2019) T. Int J Biol Macromol 129:615–633
8. Channa AM, Siyal AN, Memon SQ, Parveen S (2016) Desalin Water Treat 57:1–8
9. Das P, Linert W (2016) Coord Chem Rev 311:1–23
10. Kaczmarek MT, Zabiszak M, Nowak M, Jastrzab R (2018) Coord Chem Rev 370:42–54
11. Soomro FK, Memon SQ, Memon N (2020) Polym Bull 77:2367–2383
12. Udhayakumari D, Naha S, Velmathi S (2017) Anal Methods 9:552–578
13. Falchuk K (1998) Mol Cell Biochem 188:41–48
14. Frederickson C, Bush A (2001) Biometals 14:353–366
15. Li D, Liu L, Li WH (2015) ACS Chem Biol 10:1054–1063
16. Jiang P, Guo Z (2004) Coord Chem Rev 248:205–229

17. Domaille DW, Que EL, Chang CJ (2008) Nat Chem Biol 4:168–175
18. Park GJ, Na YJ, Jo HY, Lee SA, Kim C (2014) Dalton Trans 43:6618–6622
19. Rafighi P, Yaftian M, Noshiranzadeh N (2010) Sep Purif Technol 75:32–38
20. Ahmadpour A, Tahmasbi M, Bastami TR, Besharati JA (2009) J Hazard Mater 166:125–930
21. Ye Y, Ali A, Yin X (2002) Talanta 57:945–951
22. Tewari PK, Singh AK (2000) Fresenius J Anal Chem 367:562–567
23. Linnik RP, Zaporozhets OA (2003) Anal Bioanal Chem 375:1083–1088
24. Yan B, Worsfold PJ (1990) Anal Chim Acta 236:287–292
25. Fukuda M, Hayashibe Y, Sayama Y (1995) Anal Sci 11:13–16
26. Hutton EA, van Elteren JT, Ogorevc B, Smyth MR (2004) Talanta 63:849–855
27. Lidén C, Skare L, Lind B, Nise G, Vahter M (2006) Contact Dermatitis 54:233–238
28. Kumar ARSS, Piana F, Mičušík M, Pionteck J, Banerjee S, Voit B (2016) Mater Chem Phys 182:237–245
29. Jian-feng G, Chang-jun H, Mei Y, Dan-qun H Jun-jie L, Huan-bao F, Hui-bo L, Ping Y (2016) Anal Methods 8, 5526–5532
30. Saadman A, Md Mhahabubur R, Ismet B, Douglas RP, Md Alamgir H (2020) Polyhedron 187:114681–114681
31. Kułaczkowska AD, Bartyzel AJ (2011) Mol Struc 87:997
32. Chetana PR, Srinath BS, Somashekar MN, Policegoudra RS (2016) J Mol Struct 352:1106
33. Bullock JJ, Tajmir-Riahi HA (1978) J Chem Sot 36
34. Taqui Khan, MM, Vijay Sen Reddy V (1986) Inorg Chem 25, 208
35. Puratchikody A, Doble M (2007) Bioorg Med Chem 15:1083
36. Shalini K, Sharma PK, Der KNJ (2010) Chem Sin 36:1
37. Song EJ, Kang J, You GR, Park GJ, Kim Y, Kim SJ, Kim C, Harrison RG (2013) Dalton Trans 42:15514
38. Gong ZL, Ge F, Zhao BX (2011) Sens Actuators B 159:148–153
39. Azadbakht R, Keypour H (2012) Spectrochim Acta, Part A 85:293–297
40. Singh K, Raparia S (2018) J anal pharm res 7:4
41. Hosseini M, Ghafarloo A, Ganjali MR, Faridbod F, Norouzi P, Niasari MS (2014) Sensor Actuat B 198:411–415
42. Choi YW, Park GJ, Na YJ, Jo HY, Lee SA, You GR, Kim C (2014) Sensor Actuat B 194:343–352
43. Hosseini M, Vaezi Z, Ganjali MR, Faridbod F, Abkenar SD, Alizadeh K, Salavati-Niasari M (2010) Spectrochim Acta, Part A 75:978–982
44. Saadman A, Md Mhahabubur R, Ismet B, Douglas RP, Alamgir H (2020) Polyhedron 187, 114681
45. Ganesan JS, Sepperumal M, Ayyanar S (2020) Spectrochim. Acta Part A 226, 117613
46. Celestina JJ, Tharmaraj P, Jeevika A, Sheela CD (2020) Microchem J 155, 104692
47. Liu H, Zhao H, Tong Z, Zhang Y, Lan B, Wang J (2017) Sensors Actuators B Chem 239:511–514
48. Soong EJ, Kang J, You GR, Park GJ, Kim Y, Kim S, Kim C, Harrison RG (2013) Dalton Trans 42:15514–15520
49. Patel UB, Mehta VN, Kumar MA, Kailasa SK (2013) Res Chem Intermed 39:771–779
50. Kim SY, Lee SY, Jung JM, Kim MS, Kim C (2017) Inorganica Chim Acta 7:17650